Advances in Science and Technology Research Journal

Advances in Science and Technology Research Journal, 2026, 20(3), 98–110
https://doi.org/10.12913/22998624/213791
ISSN 2299-8624, License CC-BY 4.0

Received: 2025.10.08
Accepted: 2025.11.31
Published: 2026.02.01

Photogrammetric and light detection and ranging data analysis for digital terrain modeling in linear infrastructure

Marcin Bilski[1*], Anna Małek[1]

[1] Institute of Civil Engineering, The Faculty of Civil and Transport Engineering, Poznan University of Technology, Piotrowo 5 St., 61-138 Poznan, Poland
* Corresponding author's e-mail: marcin.bilski@put.poznan.pl

ABSTRACT

In the article, elevation data along the axes of a dirt road and an asphalt road in flat terrain were compared. For this purpose, data obtained from airborne laser scanning and from a photogrammetric survey using an unmanned aerial vehicle were used. The acquired data, in the form of a 1 × 1 m grid of terrain elevation points, were applied to create a digital terrain model in the form of a grid or triangles. The grid of elevation points was also resampled to resolutions of 2 m, 5 m, and 10 m. The analyses performed showed very good agreement of the acquired measurement data in the case of the asphalt road (particularly for grids with resolutions up to 5 m). Due to the uneven surface of the dirt road, photogrammetric data and the digital terrain model based on triangles provided a better representation of its terrain. For elevation differences between ALS and UAV data along road centrelines, the gravel road showed higher errors (*RMSE* from 0.09 m to 0.13 m) than the asphalt road (*RMSE* 0.04 m). The study introduces a new comparative workflow that provides a practical solution for linear infrastructure designers, supporting the selection of appropriate data sources and spatial resolutions depending on the project characteristics.

Keywords: UAV, LiDAR, photogrammetry, point cloud, DTM, linear infrastructure.

INTRODUCTION

Modern technologies for acquiring and processing geospatial data enable precise support of design processes, particularly for linear structures such as roads and railway lines. Remote sensing methods make it possible to accurately represent both the terrain topography and anthropogenic features (such as buildings, infrastructure, or vegetation cover), while simultaneously reducing the scope of fieldwork. The term remote sensing encompasses measurement techniques that allow the collection of information about objects, phenomena, and processes without direct physical contact with the investigated surface or object. Among remote sensing techniques, photogrammetry and laser scanning (light detection and ranging – LiDAR) play a key role [1, 2].

Photogrammetry using unmanned aerial vehicles (UAVs) and structure-from-motion (SfM) algorithms enables the generation of high-resolution geospatial products. The most commonly obtained outputs include orthophotomaps (terrain surface images free from geometric distortions), digital terrain models (DTM – representing the topography of the ground surface after removing above-ground objects) and digital surface models (DSM – which include the elevation of all elements such as vegetation and buildings. The quality of the results depends on various factors such as flight altitude, image overlap, sensor resolution, camera calibration, and the number and distribution of ground control points (GCPs) [3–8]. Properly conducted UAV photogrammetry can achieve horizontal and vertical accuracies of a few centimetres, comparable to GNSS – RTK (Global Navigation Satellite System - Real-Time Kinematic) measurements, where the error reaches approximately 2 cm horizontally and 4 cm vertically [9, 10]. Several studies [4, 11–14] have confirmed that UAV photogrammetry ensures high measurement accuracy even with a limited

number of GCPs. For example, a low-cost UAV mission achieved *RMSE* (root mean square error) below 5 cm horizontally and 6 cm vertically [11]. Such accuracy enables the creation of maps at scales up to 1:200 with a contour interval of 30 cm, suitable for infrastructure design. Other studies [4, 12] indicated that using only three to seven GCPs, alternately placed along both sides of the road, provides vertical *RMSE* values below 6–8 cm. UAVs equipped with RTK-enabled GNSS receivers can even achieve comparable accuracy without GCPs, typically 1–3 cm horizontally and 4–7 cm vertically [13, 14]. Although GCPs are still recommended to ensure vertical control, minimizing their number is particularly advantageous when mapping large or inaccessible areas.

Light detection and ranging (LiDAR) provides dense three-dimensional point clouds by measuring the time of flight of laser pulses reflected from surfaces. Depending on the measurement platform, LiDAR technology can be categorized as satellite laser scanning (SLS), airborne laser scanning (ALS), UAV-borne laser scanning (ULS), mobile laser scanning (MLS), and terrestrial laser scanning (TLS) [15–17]. Each of these techniques offers a different balance between accuracy, point density, range, and cost [18–20]. Satellite laser scanning (SLS) is mainly applied in large-scale studies such as spatial and environmental planning. Although it provides global coverage, its practical use is limited by low spatial resolution and sensitivity to atmospheric conditions [21–24]. In contrast, ALS offers greater flexibility in flight planning and data acquisition. It provides higher point densities and vertical accuracy between 2–15 cm, depending primarily on flight altitude, sensor characteristics, and land-cover type [24–28]. The rapidly developing UAV-borne laser scanning (ULS) technology can produce exceptionally dense point clouds with vertical accuracies between 2–10 cm [29–35]. Mobile laser scanning (MLS), performed from ground vehicles, achieves very high precision (errors below 2.5 cm) and generates extremely dense datasets, ranging from several thousand to over 30 000 points/m². It is ideal for detailed mapping of road and railway corridors [36–38]. Terrestrial laser scanning (TLS), although less mobile, offers millimetre-level precision and is commonly used for high-detail documentation and deformation analysis of buildings, bridges, and other engineering structures [39–41]. The main parameters and application ranges of different LiDAR data acquisition techniques are compared in Table 1.

In engineering practice, hybrid approaches are increasingly common, combining UAV photogrammetry and LiDAR data to enhance both completeness and accuracy [19, 39, 42, 43]. Photogrammetry offers high-resolution imagery and flexibility at low cost, while LiDAR provides dense, accurate point clouds and the ability to penetrate vegetation, which is crucial in forested or mountainous terrain [20].

A DTM is a fundamental data source in civil engineering design and analytical applications such as slope stability and hydrological modelling [44]. Two main forms of terrain representation are commonly used: the GRID model and the Triangulated Irregular Network (TIN) [45–47]. The GRID model represents elevation values on a regular grid, offering simple structure and compatibility with GIS tools. Approximately 90% of practical applications use this format because it supports efficient processing of large datasets [44, 48]. However, raster representation may smooth out narrow features such as ditches or embankments [49]. Two variants are distinguished: the cell-based model, where elevation represents the mean value of a cell, and the node-based model, where it corresponds to grid node intersections [50]. In contrast, the TIN model represents the terrain using irregular triangulation, usually based on Delaunay algorithms and structural lines. This allows flexible point distribution and accurate representation of sharp terrain features through breaklines [51, 52]. Although computationally more demanding, TIN provides superior accuracy in representing slopes, embankments, and other linear features relevant to engineering design [48, 49]. In linear infrastructure projects, such as roads or railways, accurate terrain representation is essential for designing the longitudinal profile, cross-sections, slope geometry, and drainage systems [49, 53, 54]. Comparative analyses show that TIN models better represent terrain variability, while GRID models remain advantageous for hydrological analyses where regular grid structures simplify flow modelling [49, 55]. In practice, hybrid approaches are used: TIN models are created for geometric design, while GRID models support further analytical computations [48, 53].

Various measurement methods are currently available for acquiring data on terrain surface morphology. The resulting datasets differ in accuracy, resolution, and susceptibility to interference. These

Table 1. Comparison of LiDAR data acquisition techniques [15–41]

Technique	Platform type	Typical point density (pts/m²)	Vertical accuracy (cm)	Cost	Typical applications
SLS	Satellite	<1	20–100	Very high	Regional and global mapping
ALS	Aircraft	2–5	2–15	High	Regional and urban terrain mapping
ULS	UAV	50–400	2–10	Moderate	Detailed topography and infrastructure mapping
MLS	Vehicle	5 000–30 000	1–3	High	Road and railway pavement analysis
TLS	Tripod (static)	> 10 000	<2	Moderate	High-precision building and object inspection

data can be processed in several ways to generate a digital elevation model (DEM). In the literature, two dominant forms of DEM representation are emphasized: the regular GRID structure and the triangulated irregular network (TIN) (Figure 1). These approaches vary in both terrain representation accuracy and analytical potential [48, 49]. This study aimed to assess the differences in terrain elevation resulting from the DEM generation method (GRID and TIN) and the data acquisition source (ALS and UAV). In engineering and design applications, the precision of terrain representation is important, but so are computational efficiency, data volume, and processing time. In linear infrastructure projects (e.g., roads or railways), spatial data are typically acquired from dedicated surveying campaigns carried out for design purposes. These are typically based on field measurements. For smaller projects, only characteristic points required for design are often measured. Increasingly, there is also potential to use ALS (airborne laser scanning) data from open-access sources and UAV-based photogrammetry. Such data can significantly improve the density and completeness of elevation information, enhancing the accuracy of project models. However, a larger data volume increases processing time, file size, and computational load, requiring a balance between accuracy and technical or organizational efficiency [53, 55]. Therefore, the authors attempted to evaluate which data sources and modelling methods are more suitable for specific design applications.

RESEARCH PROBLEM

Considering that open ALS (airborne laser scanning) data are available in a 1 × 1 m GRID format [57], this study investigates the potential of such data to serve as an alternative to UAV-based photogrammetric measurements. Two road sections with contrasting characteristics were selected for analysis: (1) a dirt road, representing a case where natural terrain conditions dominate and elevation changes occur over short distances, and (2) an asphalt road, representing a surface shaped and levelled during construction, with minimal height variation. The study addresses two main research questions:

- Can ALS-derived GRID data provide accuracy comparable to UAV photogrammetry for different types of road surfaces?
- Does the TIN model outperform the GRID model in representing terrain irregularities, particularly for unpaved (dirt) roads?

We hypothesize that the TIN model will more accurately capture irregular and natural surfaces such as dirt roads, whereas both GRID and TIN will perform similarly for smooth, asphalted surfaces. The two selected sites represent typical conditions encountered in linear infrastructure projects (from naturally shaped terrain to road surfaces formed through construction) providing a balanced basis for comparing model performance under contrasting topographic conditions.

RESEARCH METHODOLOGY

In this study, two road sections (Figure 2) located in flat terrain were analysed. Data for these sites were obtained from an open-access ALS database [54] and from a low-cost UAV photogrammetric flight carried out during the summer season. For the analysis, two areas were selected:

- Area 1 – a dirt road section located in the Pobiedziska commune, Poznań County, with a total length of 400 m, and
- Area 2 – a paved urban street section within the administrative boundaries of the city of Poznań, with a total length of 200 m.

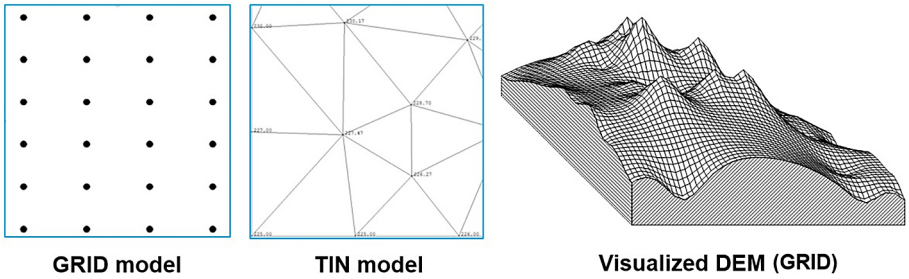

Figure 1. Graphical interpretation of the GRID, TIN, and DEM models (based on [56])

The ALS data, available from the national geodetic and cartographic resource [54], were downloaded in ESRI GRID format and converted to ASCII XYZ format. These ALS datasets are characterized by a point density ranging from 4 to 20 points/m², with a DEM resolution of 1 × 1 m. The second source of data was a DJI Mavic Air 2 unmanned aerial vehicle (UAV), whose technical specifications are presented in Table 2. The UAV photogrammetric survey was conducted during the summer period under comparable atmospheric conditions to ensure measurement consistency. For both study areas, a temporary photogrammetric control network was established, consisting of 8 ground control points (GCPs) for Area 1 and 12 GCPs for Area 2. The GCPs were implemented as black-and-white checkerboard targets measuring 0.5 × 0.5 m. The photogrammetric image alignment carried out in the software achieved an accuracy of about 3 cm for the control points and 8 cm for the check points. The coordinates of the GCPs were measured using a mobile GNSS receiver operating with GPS and GLONASS satellite data, allowing for positional accuracy of ±2 cm horizontally (axes X and Y) and ±5 cm vertically (axis Z). All datasets were referenced to the PL-ETRF2000 horizontal coordinate system and the PL-EVRF2007-NH vertical system. The acquired images were processed to create orthophotomaps and Digital Terrain Models (DTMs) using Agisoft photogrammetric software, which operates based on the Structure from Motion (SfM) technique [7]. This method enables the creation of a 3D model from a series of overlapping 2D images. As a result, DTMs were generated for both areas in GRID format, exported as ASCII XYZ files with an elevation point resolution of 1 × 1 m. To assess the influence of data resolution on the resulting DTM, the point grids were subsequently resampled to resolutions of 2 × 2 m, 5 × 5 m, and 10 × 10 m. Using CAD software (Autodesk Civil 3D), additional DTMs were created for both study areas based on the ASCII XYZ datasets with resolutions of 1 × 1 m, 2 × 2 m, 5 × 5 m, and 10 × 10 m. The final stage involved generating terrain profiles along the horizontal road axes. In total, 12 variants were developed for each road: six based on ALS data and six based on UAV data. These were derived from the following DTM configurations:

- GRID 1 × 1 m,
- TIN based on 1 × 1 m GRID,
- TIN based on 2 × 2 m GRID,
- TIN based on 5 × 5 m GRID, and
- TIN based on 10 × 10 m GRID.

The lower-resolution grids were generated directly from the original 1 × 1 m GRID by systematic subsampling. Every n-th point (corresponding to 2 m, 5 m, and 10 m spacing) was selected to create the reduced-density datasets. The 1 × 1, 2 × 2, 5 × 5, and 10 × 10 m grid sizes were chosen to provide a representative range of resolutions for evaluating the impact of data density on terrain model accuracy. Statistical analyses of the measurement results were performed using the Statistica software package. In Autodesk Civil 3D, the generation of TIN models from GRID data was performed using the Delaunay triangulation algorithm, which connects grid points into triangles forming a continuous terrain surface model [55]. In order to avoid the influence of vegetation and surface obstacles on point cloud filtering, the elevation profiles were extracted along the centreline for roads. In the case of a dirt road, the road centreline was defined by the difference in elevation between the right and left wheel tracks. Figure 3 presents the flowchart of the research process.

RESULTS AND ANALYSIS

Figures 4–7 present the terrain elevation profiles along the road axes for the analysed areas,

(a)

(b)

Figure 2. Photographs of the study areas: Area 1 – dirt road (UAV image) (a), Area 2 – asphalt pavement (view presented as a point cloud)

created using the data acquired according to the methodology described in Section 3. The comparative analysis of the longitudinal profiles for the two study areas (Area 1 – dirt road and Area 2 – asphalt road) allows for the assessment of the consistency between digital terrain models (DTMs) generated from airborne laser scanning (ALS) and low-altitude UAV photogrammetry data. In Figures 4 and 6, the DTM is based on GRID data with a 1 × 1 m elevation point resolution, whereas

Table 2. Specification of the UAV and the camera sensor

Weight [g]	570
Accuracy of vertical flight [m]	± 0.1
Camera matrix [Mpix]	48 (effective 12)
Maximum photo resolution [pixel]	8000 × 6000
Resolution of the captured photos [pixel]	4000 × 3000
ISO	100
Focal length equivalent [mm]	24
Sensor dimensions [mm]	6.4 × 4.8 (1/2" CMOS)
Iris	f/2.8

Figures 5 and 7 present DTMs created from the same 1 × 1 m GRID data but represented as TIN models. The profiles were extracted along the road centrelines at 10 m intervals. The elevation differences were computed as ALS minus UAV, meaning that positive values indicate higher elevations in the ALS-derived model compared to the UAV model. The computed statistics for elevation readings taken every 10 m are summarized in Table 3, including:

- the number of elevation points used in the calculations (n),
- the mean elevation difference (MEAN), indicating the vertical shift between data sources,
- the median (MEDIAN), showing the central value of the distribution (less sensitive to outliers than the mean),
- the standard deviation (SD), representing the dispersion of results around the mean – lower SD values indicate better agreement between datasets,
- the mean absolute error (MAE), expressing the average magnitude of elevation differences,
- the root mean square error ($RMSE$), combining systematic and random errors into a comprehensive accuracy metric,
- the minimum and maximum values (Min, Max), representing the smallest and largest elevation differences along the profiles, enabling the identification of local extremes, and
- the linear error at 95% confidence level ($LE95\%$), calculated as $1.96 \cdot SD$, which defines the interval within which the true elevation difference is expected to fall with 95% probability,
- the coefficient of determination (R^2), describing the strength of the linear relationship between the compared elevation datasets.

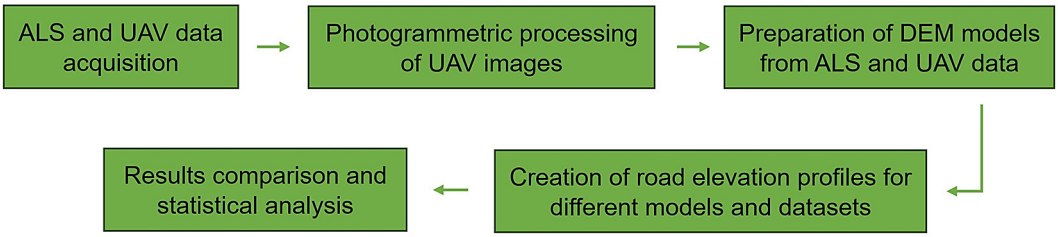

Figure 3. Flowchart of the research process

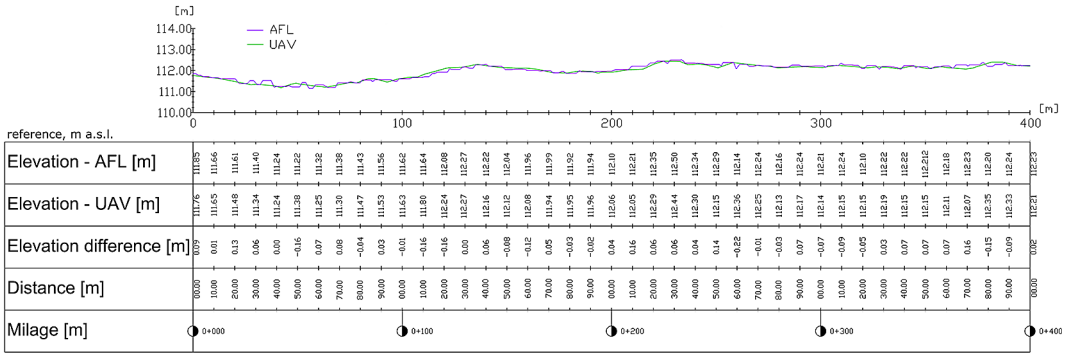

Figure 4. Elevation profile along the road centreline in Area 1 derived from a DEM with 1 × 1 m resolution

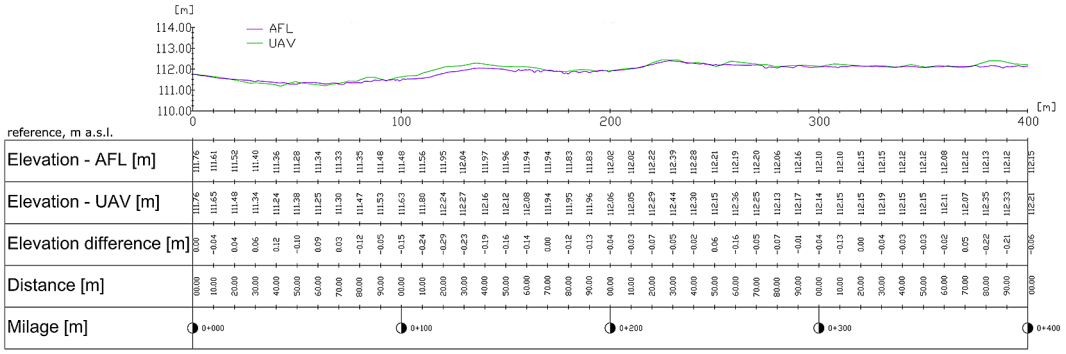

Figure 5. Elevation profile along the road centreline in Area 1 derived from a TIN-based DEM using elevation points from a 1 × 1 m grid

The mean elevation differences ranged from -0.02 m to 0.03 m, indicating very good agreement between the ALS and UAV datasets. For the dirt road (Area 1), the standard deviation of the profile based on the GRID model was ±0.11 m, while for the TIN model, it was ±0.13 m. For the asphalt road (Area 2), the standard deviation was ±0.03 m for both GRID and TIN models. These results indicate that for the dirt road, the TIN model exhibits greater elevation variability, which is a consequence of its triangulation-based structure. The TIN model captures local terrain variations more precisely, while the GRID model tends to smooth the surface through interpolation. The mean absolute error (*MAE*) was 0.06 m for the GRID model and 0.09 m for the TIN model in Area 1, and 0.03 m for both models in Area 2. Notably, the *MAE* values for the dirt road were at least twice as high as those for the asphalt road, which results from the higher level of surface detail captured in UAV data. The SfM photogrammetric reconstruction algorithms reproduce small-scale terrain features (such as ruts, local depressions, and surface irregularities) with greater precision than ALS data, which are inherently smoother due to filtering and interpolation processes. Therefore, higher *MAE* values in heterogeneous surfaces (e.g., dirt roads) should be interpreted as an indication of greater detail in UAV-derived data, rather than lower measurement accuracy. For smooth

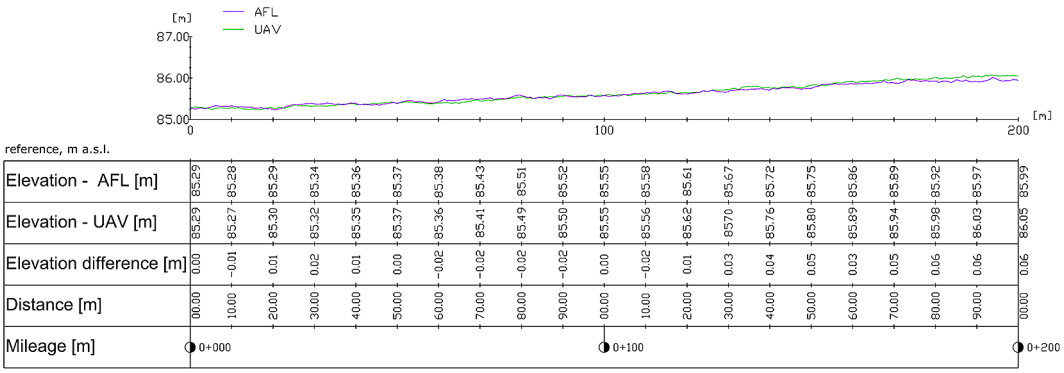

Figure 6. Elevation profile along the road centreline in Area 2 derived from a DEM with 1 × 1 m resolution

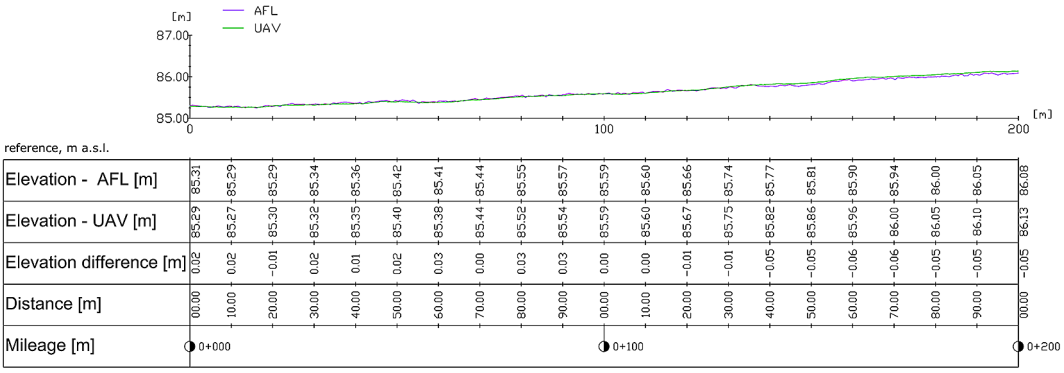

Figure 7. Elevation profile along the road centreline in Area 2 derived from a TIN-based DEM using elevation points from a 1 × 1 m grid

and homogeneous surfaces (asphalt roads), both measurement methods demonstrated very high consistency. Moreover, the variation in *MAE* values for the dirt road between GRID and TIN indicates that the GRID model smooths local extrema to a greater degree. The root mean square error (*RMSE*) values were 0.09 m for GRID and 0.13 m for TIN in Area 1, and 0.04 m for both models in Area 2. Similar to *MAE*, the *RMSE* values confirmed greater local variability in the TIN model for the dirt road, while showing strong correlation between ALS and UAV data for the asphalt road. The *RMSE* difference between the GRID and TIN models did not exceed 0.04 m for the dirt road and was 0.00 m for the asphalt road, indicating very high consistency of both terrain models for flat areas. The largest local elevation differences for the dirt road between the GRID and TIN models ranged from -0.29 m to 0.16 m, reflecting the uneven surface. For the asphalt road, the extreme values for both models were ±0.06 m. The higher differences observed for Area 1 can be attributed to the greater local variability captured by UAV photogrammetric reconstruction, which produces a more detailed elevation profile. The LE95% values were 0.22 m for GRID and 0.26 m for TIN in Area 1, and 0.07 m and 0.08 m, respectively, in Area 2. These results confirm significant variation in the datasets depending on the surface characteristics and the measurement method (ALS or UAV). In summary, the obtained results show that higher correlation between ALS and UAV data (i.e., lower *SD*, *RMSE*, and *LE*95%) was achieved for the asphalt road, due to its homogeneous and smooth surface. In contrast, the dirt road exhibited greater discrepancies because of its irregular topography. The GRID-based DTM demonstrates lower elevation variability due to interpolation, which partially smooths local irregularities, whereas the TIN model provides a more detailed representation of the actual terrain profile and is thus more sensitive to local elevation differences captured in UAV data. Consequently, the TIN model produces a wider range of elevation differences (higher *SD*, *RMSE*, and *LE*95%), which reflects the true variability of the terrain surface rather than photogrammetric reconstruction error. An *F*-test is a statistical test used to compare the variances of two or

more groups to determine if they are significantly different. The interpretation of the results depends on the *p*-value. If it is lower than the chosen significance level (e.g., 0.05), the null hypothesis of equal variances is rejected. A large *F*-value indicates greater differences between group variances. In this case, the variance comparison using an *F*-test ($p > 0.05$) showed no statistically significant difference between the GRID and TIN elevation residuals. Although the TIN model exhibited slightly higher variability in Area 1 (*SD* = 0.13 m vs. 0.11 m), this difference was not statistically significant. In Area 2, both models demonstrated identical variability (*SD* = 0.03 m), indicating consistent performance regardless of the surface modelling method. The R^2 values for the analysed cases were 0.99, indicating a good agreement between the ALS and UAV data.

Figures 8 and 9 present the elevation differences between ALS and UAV data for DTMs in TIN form, generated from GRID datasets with an original resolution of 1 × 1 m, subsequently resampled to 2 × 2 m, 5 × 5 m, and 10 × 10 m. In the calculations, absolute elevation differences were used, derived from measurements taken every 10 m along the road centerlines. For the dirt road, the mean absolute elevation difference between ALS and UAV data ranged from 0.09 m to 0.10 m, regardless of the applied grid resolution. The variability range (expressed as ±1.96·SD) extended from -0.01 m to 0.20 m for the 1 × 1 m grid, and from -0.06 m to 0.24 m for the 10 × 10 m grid, indicating a gradual increase in variability with decreasing grid resolution (larger cell size). For the asphalt surface, the elevation differences between ALS and UAV data were significantly smaller. The mean absolute elevation differences were approximately 0.03 m for grids ranging from 1 m to 5 m, while for the 10 × 10 m grid, the mean difference increased slightly to 0.05 m. The variability range for grids from 1 m to 5 m was -0.02 m to 0.08 m, and for the 10 m grid, it was -0.07 m to 0.16 m. The obtained results indicate very good agreement between ALS and UAV data in the creation of TIN-based DTMs for paved or well-graded road surfaces, particularly when using grid resolutions of up to 5 m. The homogeneous and smooth asphalt surface ensures high measurement precision for both technologies (ALS and UAV) and minimizes the impact of disturbing factors such as vegetation or surface irregularities. In the case of the dirt road, due to differences in data acquisition methods – UAV data showing locally higher elevation variability, and ALS data being more smoothed – comparable elevation differences for the TIN model were observed up to a 2 m grid resolution. It should be noted that, in the case of the analyzed data, the obtained accuracy represents the sum of measurement errors influenced by many factors, ranging from measurement conditions to alignment errors and others.

Figures 10 and 11 illustrate the elevation differences between ALS and UAV data along the analysed terrain profiles in Area 1 (gravel road) and Area 2 (asphalt road), respectively, for different grid resolutions (1 m, 2 m, 5 m, and 10 m). In both areas, finer grids (1 × 1 m, 2 × 2 m) result in the smallest elevation differences, while coarser grids (5 × 5 m, 10 × 10 m) tend to introduce greater discrepancies due to surface generalization. The differences are more pronounced in Area 1, where the unpaved road lacks uniform grading and is more exposed to natural surface irregularities. In contrast, the asphalt surface in Area 2 is well-profiled, resulting in smaller and more consistent deviations, even for the 5 × 5 m grid resolution.

Table 4 presents a comparison of the collected data regarding the number of elevation points in both study areas depending on the grid resolution. It should be noted that the 2 × 2 m grid contains approximately 75% fewer measurement points, while the 5 × 5 m grid includes about 96% fewer points than the base 1 × 1 m resolution. The 10 × 10 m grid represents only 1% of the number of points in the base 1 × 1 m dataset. The GRID

Table 3. Statistical summary of elevation differences for ALS and UAV data along road horizontal alignments (centrelines)

Area	Profile source	*n*	Mean [m]	Median [m]	*SD* [m]	*MAE* [m]	*RMSE* [m]	Min [m]	Max [m]	*LE*95% [m]	R^2
Area 1 (gravel road)	GRID	41	0.02	0.02	±0.11	0.06	0.09	-0.22	0.16	0.22	0.99
	TIN	41	-0.02	-0.02	±0.13	0.09	0.13	-0.29	0.12	0.26	0.99
Area 2 (asphalt road)	GRID	21	0.03	0.03	±0.03	0.03	0.04	-0.02	0.06	0.07	0.99
	TIN	21	0.03	0.03	±0.03	0.03	0.04	-0.06	0.03	0.08	0.99

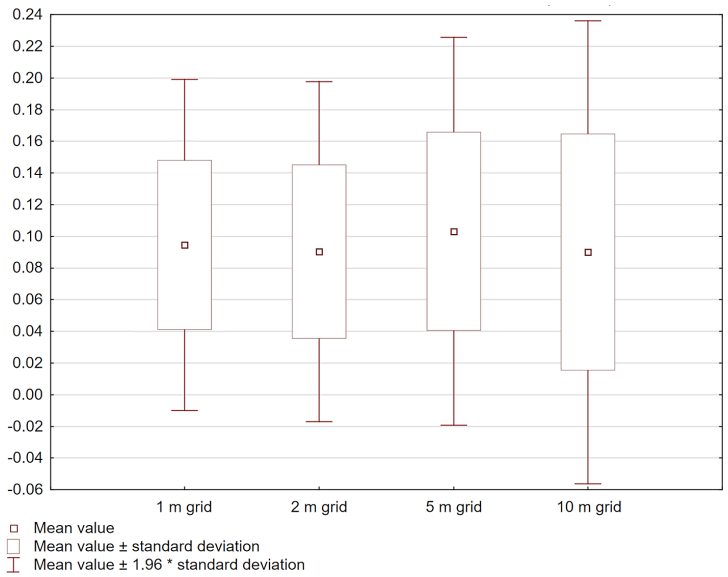

Figure 8. Comparison of elevation profiles along the road centreline in Area 1 derived from TIN-based DEMs with varying grid resolutions.

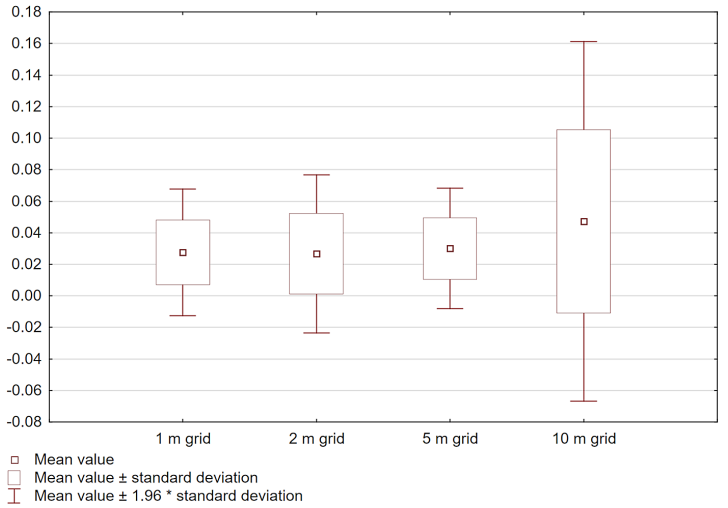

Figure 9. Comparison of elevation profiles along the road centreline in Area 2 derived from TIN-based DEMs with varying grid resolutions

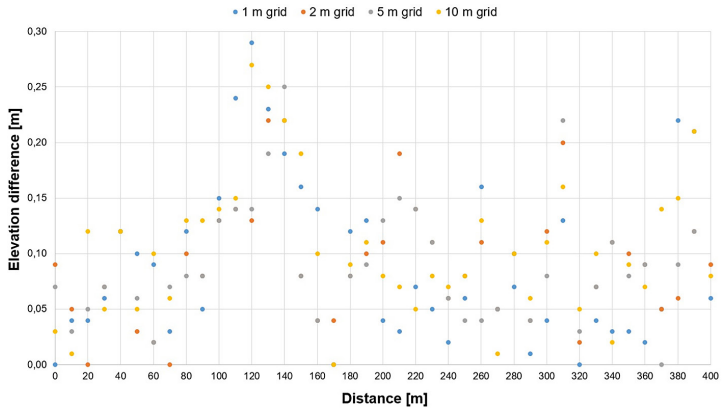

Figure 10. Elevation differences between ALS and UAV data along the analysed terrain profile in Area 1 (gravel road) for different grid resolutions (1 m, 2 m, 5 m, and 10 m)

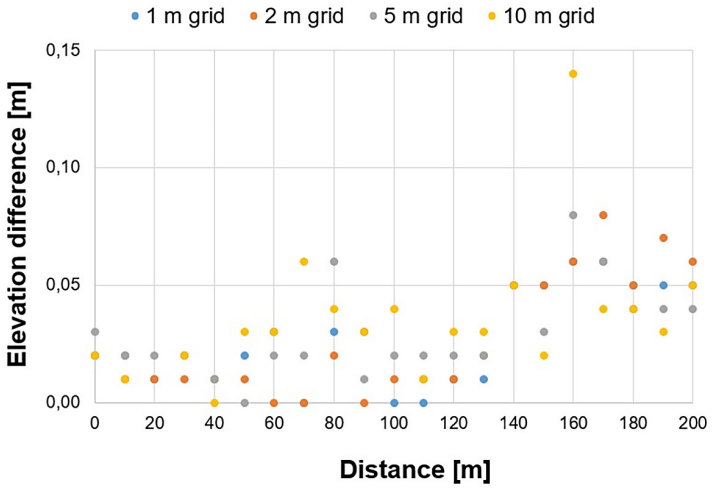

Figure 11. Elevation differences between ALS and UAV data along the analysed terrain profile in Area 2 (asphalt road) for different grid resolutions (1 m, 2 m, 5 m, and 10 m)

Table 4. Comparison of the number of elevation points for the study areas depending on the grid size

Parameter	Grid size			
Number of elevation points	1 × 1 m	2 × 2 m	5 × 5 m	10 × 10 m
Area 1	203 643	51 302	8 385	2 161
Area 2	84 708	21 177	3 431	888

Table 5. Recommended data sources and surface modelling approaches for different terrain types

Terrain type / surface	Recommended data source	Model type	Remarks
Smooth, homogeneous (e.g. asphalt road, flat area)	ALS	GRID	High consistency, efficient processing
Irregular (e.g. dirt road, ditch)	UAV photogrammetry	TIN	Better representation of local irregularities

model can be directly used in CAD-type software. The TIN model, however, requires generation. In the analysed cases, the data file size for the 1 × 1 m grid was approximately 10.000% larger than that for the 10 × 10 m grid, and similarly, the data loading time into the software was approximately six times longer.

CONCLUSION

This study compared terrain elevation profiles along two road centrelines: a dirt road and an asphalt road. Data came from ALS and UAV photogrammetry using the SfM method. The results showed high consistency between both datasets, especially for the asphalt surface. Mean elevation differences ranged from -0.02 m to 0.03 m. For the dirt road, higher values of *SD*, *RMSE*, and *LE*95% were observed. This was caused by greater surface irregularity and the higher detail captured in UAV data. The TIN model reproduced local surface variations more accurately. The GRID model produced a smoother surface and worked better in flat areas with low elevation variability. Different grid resolutions were also tested (1 ×1 m, 2 × 2 m, 5 × 5 m, 10 ×10 m). For asphalt roads, the high agreement between ALS and UAV data (mean absolute error ≈ 0.03 m) remained stable up to a 5 × 5 m grid. For dirt roads, elevation differences increased with grid size, but results were still reliable up to a 2 × 2 m grid. Reducing the resolution from 1 m to 2 m lowered the data volume by about 75%, with only a small loss of accuracy. A summary of the recommended data sources and modelling approaches for different terrain types is presented in Table 5. The obtained *RMSE* values were 0.04 m for the asphalt road and 0.09 to 0.13

m for the gravel road. The corresponding *MAE* values ranged from 0.03 m to 0.09 m. These results are consistent with previous studies on UAV and LiDAR terrain modelling [11, 12, 18, 34, 44, 55], where typical *RMSE* values were between 0.03 m and 0.10 m.

The obtained results confirm that both ALS and UAV photogrammetry can be effectively applied in high-precision geodetic and engineering analyses of linear infrastructure terrain modelling, with the choice of method and resolution depending on the characteristics of the analysed area. The present analysis is limited to flat-terrain conditions and a relatively small dataset. Therefore, potential bias related to the lack of complex topography should be acknowledged. Future research should include areas with more diverse terrain and larger datasets. Further extensions may involve integration with UAV-borne LiDAR or the application of machine learning methods for DTM error prediction. Nevertheless, the presented results provide practical guidance for designers and engineers in selecting the optimal data acquisition and processing approach for creating DEMs suited to the specific characteristics of the analysed linear infrastructure. In road earthworks, cross-sections are typically generated at regular intervals, for example every 25 meters, and earthwork volumes are calculated using the average-end area method. The obtained elevation accuracy, comparable to that achieved with GNSS RTK measurements, ensures that such small errors have a negligible effect on the calculated earthwork volumes. Both ALS and UAV data acquisition substantially reduce fieldwork time compared to traditional GNSS surveying. While a GNSS survey of a several-hundred-metre road section may take a few hours, UAV or ALS data collection for the same area can be completed within minutes, providing dense and consistent elevation information suitable for precise earthwork analyses.

REFERENCES

1. Sanecki J, editor. Teledetekcja. Pozyskiwanie danych [Remote sensing. Data acquisition]. Warszawa: Wydawnictwa Naukowo-Techniczne; 2006; 388.
2. Khorram S, van der Wiele CF, Koch FH, Nelson SAC, Potts MD. Principles of applied remote sensing. Cham (Switzerland): Springer; 2016. https://doi.org/10.1007/978-3-319-22560-9
3. Liu K, Sessions J. Preliminary planning of road systems using digital terrain models. J For Eng. 1993; 4(2): 27–32. https://doi.org/10.1080/08435243.1993.10702646
4. Tonkin TN, Midgley NG. Ground-control networks for image based surface reconstruction: an investigation of optimum survey designs using UAV imagery and SfM. Remote Sens. 2016; 8(9): 501. https://doi.org/10.3390/rs8090786
5. Wallace L, Lucieer A, Malenovský Z, Turner D, Vopěnka P. Assessment of forest structure using two UAV techniques: ALS and SfM point clouds. Forests. 2016; 7(3): 62. https://doi.org/10.3390/f7030062
6. Kwon S, Park JW, Moon D, Jung S, Park H. Smart merging method for hybrid point cloud data using UAV and LiDAR in earthwork construction. Procedia Eng. 2017; 196: 21–8. https://doi.org/10.1016/j.proeng.2017.07.168
7. Małek A. Assessment of the use of unmanned aerial vehicles for road pavement condition surveying. Roads Bridges – Drogi Mosty. 2023; 22(4): 331–45. https://doi.org/10.7409/rabdim.023.017
8. Chonpatathip S, Suanpaga W, Chantawarangul K. Utilizing unmanned aerial vehicles (UAVs) for earthwork fill height determination in road construction. Int J Geoinformatics. 2023; 19(10): 28–39. https://doi.org/10.52939/ijg.v19i9.2877
9. Eren M, Kurtulgu Z, Pirti A. Evaluation of the repeatability and accuracy of RTK GNSS under tree canopy. J Sylva Lestari. 2025; 13(2): 1110. http://doi.org/10.23960/jsl.v13i2.1110
10. Ekaso D, Nex F, Kerle N. Accuracy assessment of real-time kinematics (RTK) measurements on unmanned aerial vehicles (UAV) for direct geo-referencing. Geo-Spat Inf Sci. 2020; 23(2): 165–81. http://doi.org/10.1080/10095020.2019.1710437
11. Elkhrachy I. Accuracy assessment of low-cost unmanned aerial vehicle (UAV) photogrammetry. Alex Eng J. 2021; 60(6): 5579–90. https://doi.org/10.1016/j.aej.2021.04.011
12. Ferrer-González E, Agüera-Vega F, Carvajal-Ramírez F, Martínez-Carricondo P. UAV photogrammetry accuracy assessment for corridor mapping based on the number and distribution of ground control points. Remote Sens. 2020; 12(15): 2447. https://doi.org/10.3390/rs12152447
13. Žabota B, Kobal M. Accuracy assessment of UAV-photogrammetric-derived products using PPK and GCPs in challenging terrains: in search of optimized rockfall mapping. Remote Sens. 2021; 13(19): 3812. https://doi.org/10.3390/rs13193812
14. Niu Z, Xia H, Tao P, Ke T. Accuracy assessment of UAV photogrammetry system with RTK measurements for direct georeferencing. ISPRS

Ann Photogramm Remote Sens Spatial Inf Sci. 2024; X-1: 169–76. https://doi.org/10.5194/isprs-annals-X-1-2024-169-2024

15. Dong P, Chen Q. LiDAR Remote Sensing and Applications. 1st ed. Boca Raton: CRC Press; 2018; 220.
16. Oveland I, Hauglin M, Giannetti F, Kjørsvik NS, Gobakken T. Comparing three different ground based laser scanning methods for tree stem detection. Remote Sens. 2018; 10(4): 538. https://doi.org/10.3390/rs10040538
17. Soininen V, Hyyppä E, Muhojoki J, Luoma V, Kaartinen H, Lehtomäki M, Kukko A, Hyyppä J. Accuracy comparison of terrestrial and airborne laser scanning and manual measurements for stem curve-based growth measurements of individual trees. Sci Remote Sens. 2024; 9: 100125. https://doi.org/10.1016/j.srs.2024.100125
18. Süleymanoğlu B, Gürtürk M, Yılmaz Y, Soycan A, Soycan M. Comparison of Unmanned Aerial Vehicle-LiDAR and Image-Based Mobile Mapping System for Assessing Road Geometry Parameters via Digital Terrain Models. Transportation Research Record. 2023; 2677(1): 03611981231157730. https://doi.org/10.1177/03611981231157730
19. Kovanič Ľ, Topitzer B, Peťovský P, Blišťan P, Bindzárová Gergeľová M, Blišťanová M. Review of photogrammetric and LiDAR applications of UAV. Applied Sciences. 2023; 13(11): 6732. https://doi.org/10.3390/app13116732
20. Gaspari F, Ioli F, Barbieri F, Belcore E, Pinto L. Integration of UAV-LiDAR and UAV-Photogrammetry for Infrastructure Monitoring and Bridge Assessment. Int Arch Photogramm Remote Sens Spatial Inf Sci. 2022; XLIII-B2: 995–1002 https://doi.org/10.5194/isprs-archives-XLIII-B2-2022-995-2022
21. Vernimmen R, Hooijer A, Pronk M. New ICESat-2 satellite LiDAR data allow first global lowland DTM suitable for accurate coastal flood risk assessment. Remote Sens. 2020; 12(17): 2827. https://doi.org/10.3390/rs12172827
22. Hejmanowska B, Wężyk P, editors. Dane satelitarne dla administracji publicznej [Satellite data for public administration]. Gdańsk: Polska Agencja Kosmiczna; 2020; 1st ed.
23. Ma X, Zheng G, Xu C, Moskal LM, Gong P, Guo Q, Huang H, Li X, Pang Y, Wang C, Xie H, Yu B, Zhao B, Zhou Y. A global product of 150-m urban building height based on spaceborne lidar. Sci Data. 2024; 11: 1387. https://doi.org/10.1038/s41597-024-04059-0
24. Borowiecki I, Ślusarski M. Lotniczy skaning laserowy LIDAR miasta Krakowa (ocena dokładnościowa) [Airborne laser scanning LIDAR of the city of Kraków (accuracy assessment)]. Arch Fotogram Kartogr Teledet. 2006; 16: 69–78.
25. Arastounia M. An enhanced algorithm for concurrent recognition of rail tracks and power cables from terrestrial and airborne LiDAR point clouds. Infrastructures. 2017; 2(2): 8. https://doi.org/10.3390/infrastructures2020008
26. Martínez Sánchez J, Fernández Rivera F, Cabaleiro Domínguez JC, López Vilariño D, Fernández Pena T. Automatic extraction of road points from airborne LiDAR based on bidirectional skewness balancing. Remote Sens. 2020; 12(12): 2025. https://doi.org/10.3390/rs12122025
27. Antah FH, Khoiry MA, Abdul Maulud KN, Abdullah A. Perceived usefulness of airborne LiDAR technology in road design and management: a review. Sustainability. 2021; 13(21): 11773. https://doi.org/10.3390/su132111773
28. Zhang L, Wang J, Shen Y, Liang J, Chen Y, Chen L, Zhou M. A deep learning based method for railway overhead wire reconstruction from airborne LiDAR data. Remote Sens. 2022; 14(20): 5272. https://doi.org/10.3390/rs14205272
29. Guan S, Zhu Z, Wang G. A review on UAV-based remote sensing technologies for construction and civil applications. Drones. 2022; 6(5): 117. https://doi.org/10.3390/drones6050117
30. Zhang J, Wolek A, Willis AR. UAV-borne mapping algorithms for low-altitude and high-speed drone applications. Sensors. 2024; 24(7): 2204. https://doi.org/10.3390/s24072204
31. Wang S, Zhao Z, Liu H. Power corridor safety hazard detection based on airborne 3D laser scanning technology. ISPRS Int J Geo Inf. 2024; 13(11): 392. https://doi.org/10.3390/ijgi13110392
32. Sampath A, Irwin J, Kim M. Airborne lidar accuracy analysis for dual photogrammetric and lidar sensor pilot project in Colorado, 2019. U.S. Geological Survey Open-File Report 2024-1036. Reston (VA): U.S. Geological Survey; 2024; 22. https://doi.org/10.3133/ofr20241036
33. Kuželka K, Slavík M, Surový P. Very high density point clouds from UAV laser scanning for automatic tree stem detection and direct diameter measurement. Remote Sens. 2020; 12(8): 1236. https://doi.org/10.3390/rs12081236
34. Bartmiński P, Siłuch M, Kociuba W. The effectiveness of a UAV-based LiDAR survey to develop digital terrain models and topographic texture analyses. Sensors. 2023; 23(14): 6415. https://doi.org/10.3390/s23146415
35. Tamimi R, Süleymanoğlu B, Elashry A, Toth C. Comparative assessment of LiDAR point clouds captured using Inertial Labs RESEPI Gen-I-M2X and DJI Zenmuse L2 sensors on UAS platforms for varying terrain conditions. ISPRS Ann Photogramm Remote Sens Spatial Inf Sci. 2025; X-G: 871–8. https://doi.org/10.5194/isprs-annals-X-G-2025-871-2025

36. Yan L, Liu H, Tan J, Li Z, Xie H, Chen C. Scan line based road marking extraction from mobile LiDAR point clouds. Sensors. 2016; 16(6): 903. https://doi.org/10.3390/s16060903
37. Kaartinen H, Hyyppä J, Kukko A, Jaakkola A, Hyyppä H. Benchmarking the performance of mobile laser scanning systems using a permanent test field. Sensors. 2012; 12(9): 12814–35. https://doi.org/10.3390/s120912814
38. De Blasiis MR, Di Benedetto A, Fiani M. Mobile laser scanning data for the evaluation of pavement surface distress. Remote Sens. 2020; 12(6): 942. https://doi.org/10.3390/rs12060942
39. Małyszek HA. The case study of using photogrammetric systems and laser scanning for three-dimensional modeling of cultural heritage sites. Adv Sci Technol Res J. 2023; 17(6): 345–57. https://doi.org/10.12913/22998624/174063
40. Liu J, Azhar S, Willkens D, Li B. Static terrestrial laser scanning (TLS) for heritage building information modeling (HBIM): a systematic review. Virtual Worlds. 2023; 2(2): 90–114. https://doi.org/10.3390/virtualworlds2020006
41. Rashdi R, Martínez-Sánchez J, Arias P, Qiu Z. Scanning technologies to building information modelling: a review. Infrastructures. 2022; 7(4): 49. https://doi.org/10.3390/infrastructures7040049
42. Klapa P, Żygadło A, Pepe M. 3D heritage reconstruction through HBIM and multi-source data fusion: geometric change analysis across decades. Appl Sci. 2025; 15(16): 8929. https://doi.org/10.3390/app15168929
43. Tysiąc P, Sieńska A, Tarnowska M, Kędziorski P, Jagoda M. Combination of terrestrial laser scanning and UAV photogrammetry for 3D modelling and degradation assessment of heritage building based on a lighting analysis: case study—St. Adalbert Church in Gdansk, Poland. npj Heritage Sci. 2023; 11: 53. https://doi.org/10.1186/s40494-023-00897-5
44. Mesa-Mingorance JL, Ariza-López FJ. Accuracy assessment of digital elevation models (DEMs): A critical review of practices of the past three decades. Remote Sens. 2020; 12(16): 2630. https://doi.org/10.3390/rs12162630
45. Forkuo E. Digital terrain modeling in a GIS environment. In: XXXVII Congress – International Archives of the Photogrammetry, Remote Sensing and Spatial Information Sciences, 2008; XXXVII, Part B2; Beijing. p. 2.
46. Burrough PA, McDonnell RA. Principles of Geographical Information Systems. Oxford: Oxford University Press; 1998.
47. Weibel R, Heller M. Digital terrain modeling. In: Maguire DJ, Goodchild MF, Rhind DW, editors. Geographical Information Systems: Principles and Applications. London: Longman; 1991; 269–97.
48. Polidori L, El Hage M. Digital elevation model quality assessment methods: A critical review. Remote Sens. 2020; 12(21): 3522. https://doi.org/10.3390/rs12213522
49. Carrara A, Bitelli G, Carla R. Comparison of techniques for generating digital terrain models from contour lines. Int J Geogr Inf Sci. 1997; 11(5): 451–73. https://doi.org/10.1080/136588197242257
50. Guth PL, Van Niekerk A, Grohmann CH, Muller J-P, Hawker L, Florinsky IV, Gesch D, Reuter HI, Herrera-Cruz V, Riazanoff S, et al. Digital elevation models: terminology and definitions. Remote Sens. 2021; 13(18): 3581. https://doi.org/10.3390/rs13183581
51. Briese C, Mandlburger G, Ressl C, Brockmann H. Automatic break line determination for the generation of a DTM along the River Main. In: Bretar F, Pierrot-Deseilligny M, Vosselman G, editors. Laser scanning 2009, IAPRS. XXXVIII, Part 3/W8; 2009 Sep 1–2; Paris, France. 7–12.
52. Kumler MP. An intensive comparison of triangulated irregular networks (TINs) and digital elevation models (DEMs). Cartographica. 1994; 31(2): 1–99. https://doi.org/10.3138/TM56-74K7-QH1T-8575
53. Fellendorf M. Digital terrain models for road design and traffic simulation. In: Fritsch D, editor. Photogrammetric Week 2013. Heidelberg: Wichmann; 2013; 270–7.
54. Gu L, Lu X, Li Y, Liu P, Sun X, Liu H. Application of breakline and manual additional points in TIN modeling. Int Arch Photogramm Remote Sens Spatial Inf Sci. 2009;XXXVIII(7-C4): 346–51.
55. Yang B, Shi W, Li Q. An integrated TIN and Grid method for constructing multi-resolution digital terrain models. Int J Geogr Inf Sci. 2005; 19(10): 1019–38. https://doi.org/10.1080/13658810500391156
56. Geoportal. Digital elevation model (DEM). Available from: https://www.geoportal.gov.pl/en/data/digital-elevation-model-dem/
57. Geoportal. Available from: https://mapy.geoportal.gov.pl/imap/Imgp_2.html?gpmap=gp0
58. Autodesk Help Manual. Available from: https://help.autodesk.com/view/CIV3D/2025/ENU/?guid=GUID-D0FCED34-D68F-42D2-A6FB-14C454CA57FA